

L. PASTIEROVIČOVÁ^{1*}, L. KUCHARIKOVÁ¹, E. TILLOVÁ¹, V. ZATKALÍKOVÁ¹,
M. UHRÍČIK¹, T. LIPTÁKOVÁ¹, M. CHALUPOVÁ¹

EFFECT OF MN ADDITION ON THE CORROSION AND FATIGUE PROPERTIES OF A PROGRESSIVE SECONDARY A357 ALLOY

As the modern automotive industry is looking for lightweight alternatives to minimize car emissions and fuel consumption, recycled Al-Si alloys play a key role in achieving this due to their lightweight, high specific strength, good castability, and corrosion resistance. In contrast to many other benefits, these alloys have reduced metallurgical micropurity as a result of recycling. The most significant complication of alloys is iron contamination. Higher Fe contents cause β -Fe-intermetallic phases in the form of long and brittle platelets that negatively affect corrosion resistance and fatigue. Neutralizing elements lead to the formation of less harmful α -Fe-rich phases, therefore a positive effect on properties is also expected. For this reason, the study investigates the effect of Mn addition on the corrosion properties achieved by immersion test and potentiodynamic polarization test and fatigue of secondary AlSi7Mg0.6 secondary alloy.

Keywords: Aluminium alloys; iron contamination; manganese addition; corrosion; fatigue

1. Introduction

Regarding economic and environmental requirements, it is increasingly important to reduce vehicle weight and thus fuel consumption. To achieve this, the secondary “recycled” Al-Si alloys are widely used for the production of automotive components operating at relatively high temperatures (up to 200°C). In addition, they form the most significant part of all castings produced [1]. The combination of suitable mechanical and foundry properties enables many applications in the automotive field. However, the properties of Al-Si aluminium alloys are significantly affected by their chemical composition [2].

Secondary aluminium alloys are rich in impurities as they are made by recycling scrap, which reflects in the quality and worse mechanical properties compared to primary alloys [3,4]. However, reusing scrap to produce secondary aluminium alloys is an environmentally friendly, inexpensive process with low energy consumption. Recycling saves almost 95% of the energy needed to produce primary Al by mining from ore and produces approx. 5% of the CO₂ emissions than primary production. Therefore, secondary aluminium alloys are considered a key enabler of decarbonization [3,5].

Investigation of these alloys led to the discovery of “principal chemical elements” as they define microstructure and properties. Depending on the nature of an alloy, the same elements could play different roles. For instance, the high iron content is currently a considerable problem [3,6]. Depending on its state, iron in such alloys can have both negative and positive effects. Iron at low contents improves the high-temperature properties and thermal stability of the alloy, prevents sticking casting on the metal mould (HDPC), and also increases the strength [6-8]. Unlike, at higher contents (above 0.8% hm. Fe), iron leads to the formation of a higher amount of various types of Fe-rich intermetallic phases, whose morphology influences the properties of the casting. During the crystallization of eutectic, Al₃FeSi (β -phase) is dominant, and the growth of silicon crystals together with aluminum starts from it [7,8]. The platelet (3D)/needle-like(2D) Al₃FeSi phase is an undesirable constituent of foundry Al-Si alloy structure since cracks are easily formed on the sharp edges of the needle crystals and then propagate along its entire length thus its shape degrades other mechanical properties as strength, fatigue, fracture toughness, and ductility. Additionally, a higher porosity formation and shrinkage have also been reported as pores nucleated along the long sides of β -platelets

¹ UNIVERSITY OF ŽILINA, FACULTY OF MECHANICAL ENGINEERING, DEPARTMENT OF MATERIALS ENGINEERING, UNIVERZITNÁ 8215/1, 010 26 ŽILINA, SLOVAK REPUBLIC

* Corresponding author: lucia.pastierovicova@fstroj.uniza.s



[7-10]. In terms of corrosion resistance, since the Al_5FeSi phase is cathodic with respect to the Al- matrix no significant degradation of corrosion resistance is expected [2,11,12].

A significant problem is a complicated way of eliminating iron's negative effects resp. its removal from the alloy, therefore neutralizing elements such as Mn, Zn, Sr, and so on are added to the melt to eliminate the negative effect of Fe to a minimum [2,13]. In technical practice, the most widely used is manganese with the effect of transformation morphology of needle-like Al_5FeSi phases into a compact shape e.g. "Chinese script" or skeleton-like of $Al_{15}(FeMn)_3Si_2$ phase, therefore improvement in mechanical and corrosion properties is expected. To achieve this, the recommended ratio according to several authors is Mn : Fe = 1 : 2 [14-17]. Author Esquivel [17] reported that increasing the Mn/Fe ratio would result in increased corrosion resistance in various cast alloys containing Mn, Fe, Si, and minor additions of Mg which is also related to the work of the author Arrabal [18] that manganese reduces the cathodic effect of Fe resulting in less intense galvanic couples compared with Al_5FeSi intermetallic phase. The improvement of microstructure and corrosion resistance of the Al-Si casts is also confirmed by authors Pasternak [15] and Mikolajčik [16]. Author Mikolajčik [16] reported that the Mn addition improves the corrosion properties of A357 alloy by the presence of skeleton-like $Al_{15}(FeMnMg)_3Si_2$ phase. However, other work of Arrabal [12] reported that commonly occurring pitting corrosion is formed and propagated preferentially along all Fe-rich phases independently of additions under the same test condition of 3.5% NaCl solution for A356 alloy. Additionally, corrosion resistance is affected also by the presence of eutectic since Si is cathodic with respect to the Al-matrix, which might lead to the formation of micro-galvanic couples resulting in localized corrosion phenomena [11,18].

The fatigue life of secondary alloys is affected primarily by the presence of casting defects such as porosity and shrinkage. High porosity was also observed in the authors' Tebaldini [19] and Kuchariková [10] works, where surface and subsurface pores acted as initiation sites for cracks. Author Kucharikova [10] also investigated the effect of Mn on the fatigue life of A356 alloy and no significant effect was observed. The fatigue life of the alloy was strongly influenced by the presence of pores. However, other our research work [20] investigated the manganese addition promoting casting defects primarily pores which increased in size and number with increasing Mn/Fe ratios, therefore, the detailed effect of manganese on mechanical properties needs to be investigated comprehensively.

For this reason, the study investigates the effect of Mn addition as a neutralizing element on the corrosion and fatigue properties of a progressive secondary A357 alloy with regard to a higher Fe content.

2. Experimental material

The secondary AlSi7Mg0.6 (EN 42200, A357) alloys were used in this study. The alloys were cast by gravity casting method into the sand mold in the form of bars with 20 mm in diameter and length of 300 mm in UNEKO, LtD (CZ) company. The chemical composition of experimental alloys is shown in TABLE 1. The alloy B was intentionally alloyed by a higher Mn content to obtain the ratio of Mn/Fe = 0.55 to investigate its effect on corrosion and mechanical properties.

This alloy is mostly used in the automotive industry, extensively used in structural automotive applications such as blocks, cylinder heads, suspension systems, and so on since the alloy is characterized by very good castability and specific strength, good corrosion, and fatigue resistance [21].

3. Experimental procedure

Metallography specimens were sectioned from the as-cast bars in transversal and longitudinal directions. The samples (18×10 mm) were mechanically ground, polished, and standard prepared for metallographic observations. After final polishing, the samples were etched with a standard HF reagent and then studied using a light optical microscope Neophot 32. The intermetallic phases were identified using a scanning electron microscope VEGA LMU II equipped with energy-dispersive X-ray spectrometer (EDX) Bruker Quantax.

After metallographic evaluation, the corrosion and fatigue tests were performed. From the as-cast bars were sectioned samples for corrosion tests with a diameter of 18 and length of 10 mm, identical as for microstructure evaluation. Corrosion testing of the alloys consists of two basic tests – immersion and potentiodynamic polarization testing. For the immersion testing the samples were immersed in 3.5% NaCl solution for 3 weeks at $20 \pm 2^\circ C$ while the solution and samples were constantly monitored. The samples were weighed before and after the test. Weight losses were used to calculate corrosion rates. After weighing, the corroded surface of the samples was observed by Leica S9D and then the cross-section was observed by light microscopy with the use of Neophot 32 optical microscope. Potentiodynamic polarization testing was chosen to evaluate the electrochemical corrosion characteristics. Each specimen was degreased in ethanol and dried before testing. Measurements were performed in the 0.5 M NaCl at $20 \pm 2^\circ C$, using laboratory potentiostat VSP Biologic SAS. The applied potential ranged from -200 mV to +300 mV. The range of potentials was set with respect to the open circuit potential (OCP) and the scan rate was 0.2 mV/s. The measured data were analyzed by the Tafel extrapolation

TABLE 1

Chemical composition of experimental alloys [wt.%]

AlSi7Mg0.6	Si	Zn	Mg	Fe	Cu	Mn	Ti	Sb	Sn	Al
Alloy A	7.374	0.069	0.477	0.750	0.017	0.071	0.121	0.007	0.004	Bal.
Alloy B	7.252	0.007	0.501	0.728	0.014	0.402	0.120	0.007	0.004	Bal.

method and the values of corrosion potential E_{corr} and corrosion current density i_{corr} were obtained using EC Lab V10.34 software [11].

Specimens used for fatigue testing under rotating bending loading were prepared according to the STN 42 0363 standard with dimensions per Fig. 1. The fatigue testing was performed on an experimental device at different stress levels with a loading frequency of 30 Hz, cycle asymmetry ratio $R = -1$ at room temperature $T = 22 \pm 1^\circ\text{C}$. The fatigue life of the experimental alloys was tested on total of 15 test specimens and the results were summarized in the form of S-N curves. Fatigue testing was terminated at $N = 5 \times 10^6$ cycles as requested by the manufacturer UNEKO, LtD. [10,11].

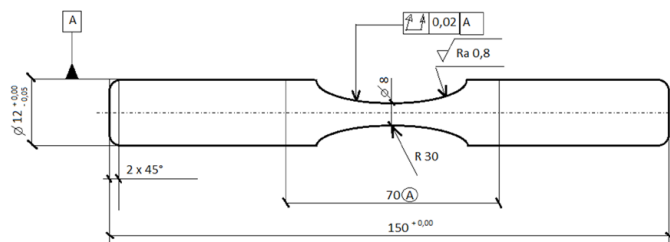


Fig. 1. Dimensions (mm) of the experimental specimens for fatigue testing

4. Results and discussion

4.1. Microstructure comparison

The representative microstructures of experimental materials are documented in Fig. 2. The microstructure of the secondary A357 cast alloy (Fig. 2) is determined by a binary Al-Si phase diagram and consists of α (Al)-matrix, eutectic (E) and various

types of intermetallic phases based on Fe, Mg, and Mn, depending on the exact chemical composition. From metallographic evaluation (Fig. 2) can be seen that both experimental materials have a comparable microstructure.

The dominant phases were based on Fe, which higher presence is a result of recycling. From these Fe-rich phases, preferentially plate-like sharp Al_5FeSi phases were observed in alloy A [10]. However, in alloy B these plate-like Al_5FeSi phases are observed as relatively shorter, less occurring, and segmented due to the addition of Mn as also reported by Bolibruchová [9] and Kuchariková [10]. The Mn addition also resulted in the presence of the $\text{Al}_{15}(\text{FeMnMg})_3\text{Si}_2$ phase in the form of Chinese script or skeleton-like in alloy B [14-16]. From the Mg-based phases were observed in the structures of both experimental materials the $\text{Al}_{15}(\text{FeMg})_2\text{Si}_2$ phases in the form of skeleton-like and the Mg_2Si phase in the form of Chinese script [22].

The effect of manganese on the Al_5FeSi phase was confirmed not only by metallographic observation of the structure but also by quantitative analysis software NIS Elements where the porosity was also evaluated due to possible increased pore formation caused by higher Mn content [20]. The results of 150 measurements are reported in TABLE 2.

From the metallography observation in Fig. 2 and quantitative analysis in TABLE 2 is obvious, that the manganese influence on Al_5FeSi phases and porosity is confirmed. The average porosity of alloy B increased by almost 20% corresponding also to previous works [10,20]. The length of Al_5FeSi plate-like phases is reduced by 53% associated with the transformation to $\text{Al}_{15}(\text{FeMnMg})_3\text{Si}_2$ skeleton-like phases (Fig. 2) [14-16]. After Mn addition the average surface ratio of $\text{Al}_{15}(\text{FeMnMg})_3\text{Si}_2$ phases occurred in the number of 8%. This is also related to the reduced appearance of Al_5FeSi phases, where the area ratio of these phases decreased by 68%.

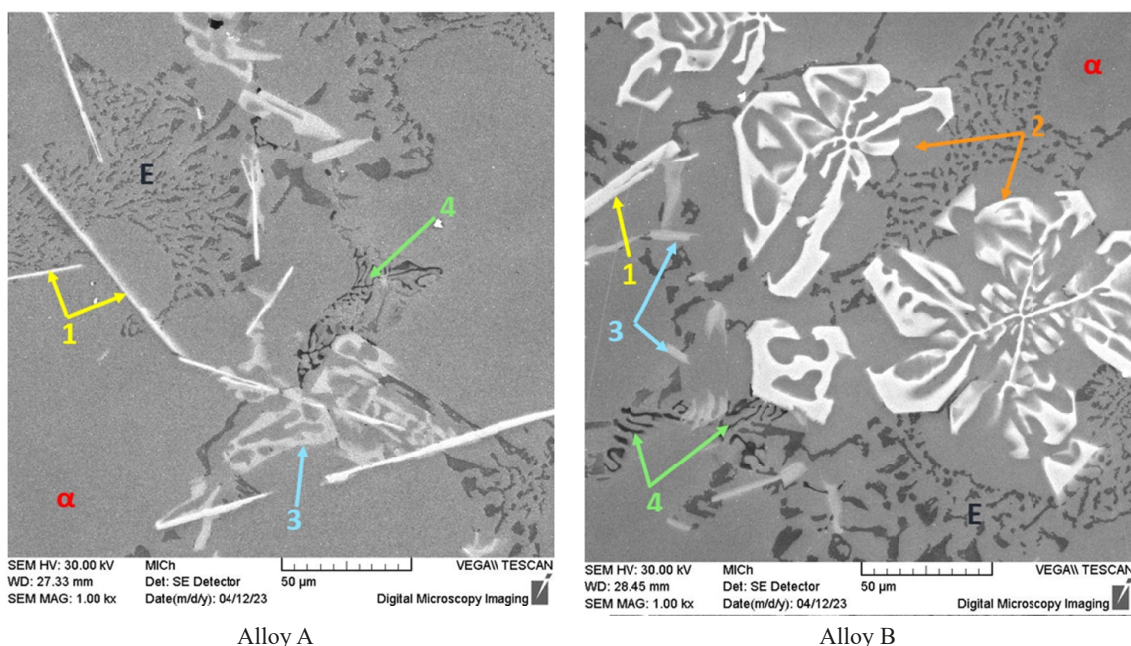


Fig. 2 Microstructure of experimental A357 alloys: α – Al(Si) matrix; E – eutectic; 1 – Al_5FeSi ; 2 – $\text{Al}_{15}(\text{FeMnMg})_3\text{Si}_2$; 3 – $\text{Al}_{15}(\text{FeMg})_2\text{Si}_2$; 4 – Mg_2Si ; etch. 0.5% HF, SEM

Results of quantitative analysis by the software NIS Elements on metallographic samples

A357	Quantification of Porosity			Quantification of Fe-rich phases								
	Pore Surface Ratio [%]			Length of Al ₅ FeSi phases [μm]			Al ₅ FeSi area surface ratio [%]			Al ₁₅ (FeMnMg) ₃ Si ₂ area surface ratio [%]		
	Min	Max	Average	Min	Max	Average	Min	Max	Average	Min	Max	Average
Alloy A	0.60	6.3	2.60	7.89	142.84	43.83	1.30	3.9	2.20	—	—	—
Alloy B	1.1	6.6	3.10	4.1	53.85	20.28	0.30	1.10	0.70	1.8	10.7	8.0

4.2. Results of immersion corrosion test

The specimens of the experimental alloys were immersed in the 3.5% NaCl solution at 20°C for three weeks. Corrosion attack was evaluated visually by light optical microscopy. A first visual evaluation (Fig. 3) revealed no major differences in the corrosion properties of the tested experimental alloys. Pitting corrosion was observed almost equally for both A357 alloys. Therefore, no positive effect of manganese content on corrosion behavior was identified, and the surface appearance and corrosion mechanisms were identical. However, the higher presence

of Fe-rich phases in alloy B (TABLE 2) increased tendency to corrosion attack.

More detailed observation of corrosion attack was possible in the cross-sections of the samples, as shown in Fig. 4. In both alloys, corrosion pits initiated and propagated deeper into the material through locations of eutectic and Fe-rich phases which correlate with the results in the literature [15-18]. Based on these observations it can be stated that the corrosion propagated deep into the material without being influenced by the manganese content since the Al₁₅(FeMnMg)₃Si₂ skeleton-like phases were also preferably attacked.

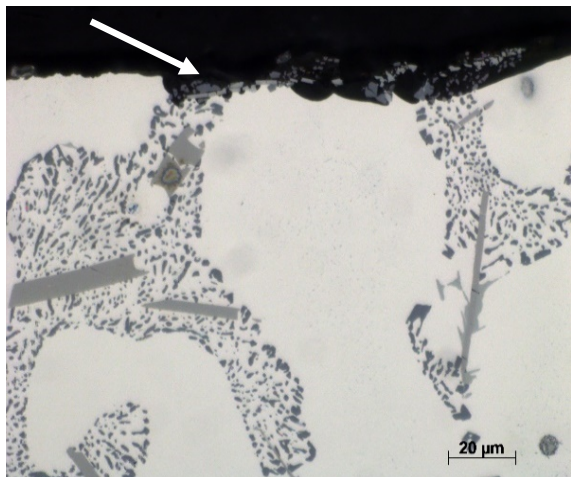


Alloy A

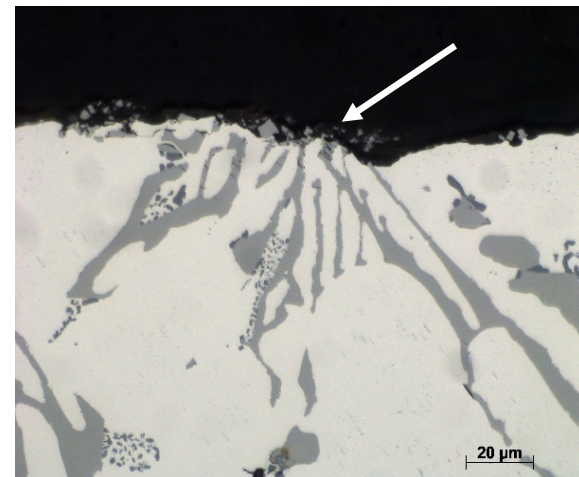


Alloy B

Fig. 3. Corrosion characteristics of the A357 experimental alloys after the immersion test



Alloy A



Alloy B

Fig. 4. Corrosion attack on A357 experimental alloys in transversal section

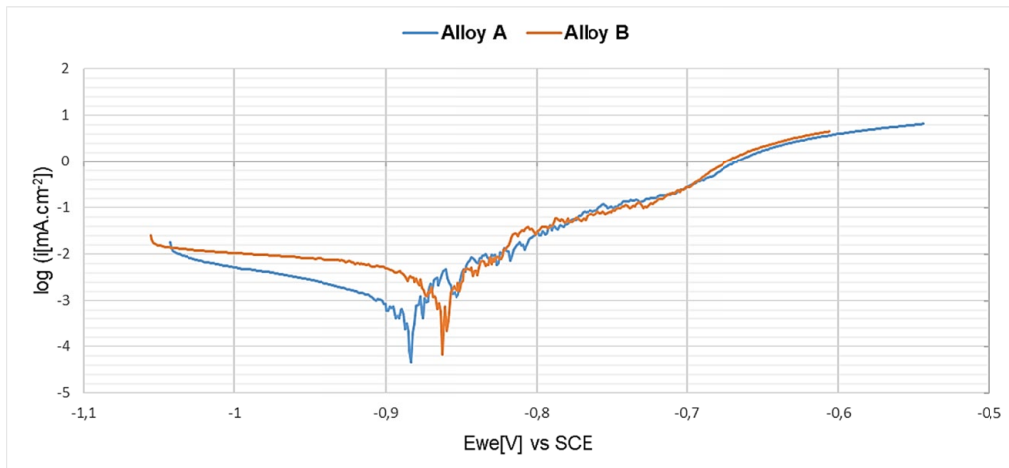


Fig. 5. Potentiodynamic polarization curves of the experimental materials in 0.5 M NaCl solution

A significant change in the corrosion resistance due to the higher manganese content of the A357 alloy was also not observed by potentiodynamic polarization tests (Fig. 5). A change in the corrosion characteristics obtained by the potentiodynamic measurements performed in 0.5 M NaCl solution is observed with respect to the Fe and Mn/Fe content in the experimental alloys. The experimentally obtained potentiodynamic curves are given in Fig. 5 and the measured corrosion characteristics are in TABLE 3. In the case of alloy B a slight shift of the E_{corr} potential to a more positive value is visible. Even when this assumes a higher thermodynamic stability of the alloy, such a small difference can be considered as negligible. However, the corrosion current density i_{corr} of alloy B is notably higher, which means, that the corrosion process is characterized by higher electric current indicating lower corrosion resistance. The corrosion rate (TABLE 3) was calculated from the weight decrease of the specimens during the immersion test. It can be seen that the corrosion rate of the alloy B is more than double that of alloy A indicating much higher corrosion kinetics of the alloy with higher Mn content.

TABLE 3

Corrosion characteristics of the A357 experimental alloys

AlSi7Mg0.6	E_{corr} [mV]	i_{corr} [$\mu\text{A}/\text{cm}^2$]	r_{corr} [mm/year]
Alloy A	-883.065	0.069	0.011
Alloy B	-863.774	1.676	0.027

Despite the fact that authors [15-18] report improved corrosion resistance due to manganese, this was not confirmed in our case as manganese caused an increase of $\text{Al}_{15}(\text{FeMnMg})_3\text{Si}_2$ phases in the alloy through which the corrosion spread further into the material.

4.3. Results of fatigue tests

The obtained results of fatigue tests are illustrated in Fig. 6. From the measured S-N curves it can be observed, that both

alloys have very similar fatigue behavior. Alloy B with Mn addition achieved a slight increase in fatigue life mainly in the region of higher stress amplitudes. This may be related to the presence of shorter Al_3FeSi plate-like phases in alloy A, which split the matrix and promote fatigue crack initiation. However, due to the severe porosity of the material, the S-N dependence is characterized by a high scatter of results indicating that the fatigue performance is determined more by the defects than by the microstructure constituents [10,20].

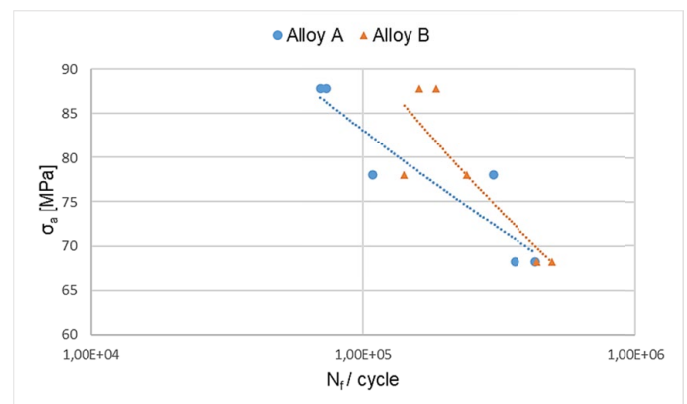


Fig. 6. The S-N curves of A357 experimental materials

Fractographic analysis in Fig. 7 revealed that the character of the fracture surfaces of the experimental materials is comparable. The surface and near-surface pores were identified as fracture initiation sites. The presence of a higher number of initiation places in specimens with higher Fe content correlates with the results of the porosity ratio in TABLE 3.

The fatigue fractures in Fig. 8 are characterized by the transcrystalline fatigue fracture of an Al-matrix with presence of typical striations. The final fracture is characterized by transcrystalline ductile fracture of a matrix with dimple morphology. The Fe-rich phases were present in both fatigue and static regions, however, they did not play a key role in crack initiation and propagation. These results correlate with the statement of Kuchariková [10] and Mikołajczak [23].

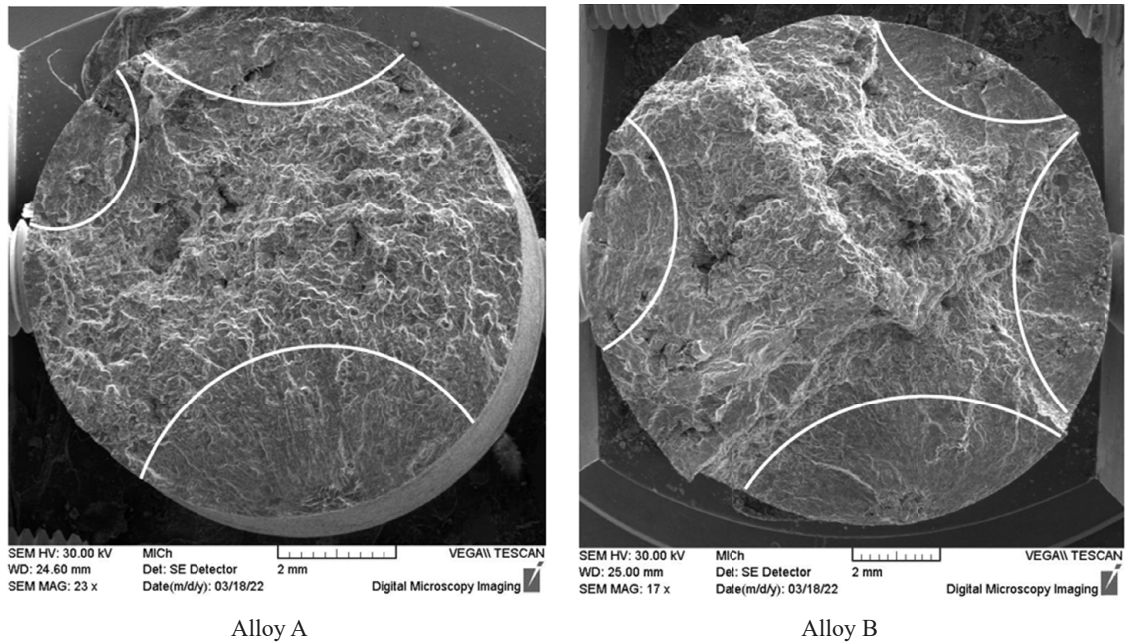


Fig. 7. Fractography analysis of fatigue fracture at 78 MPa, SEM

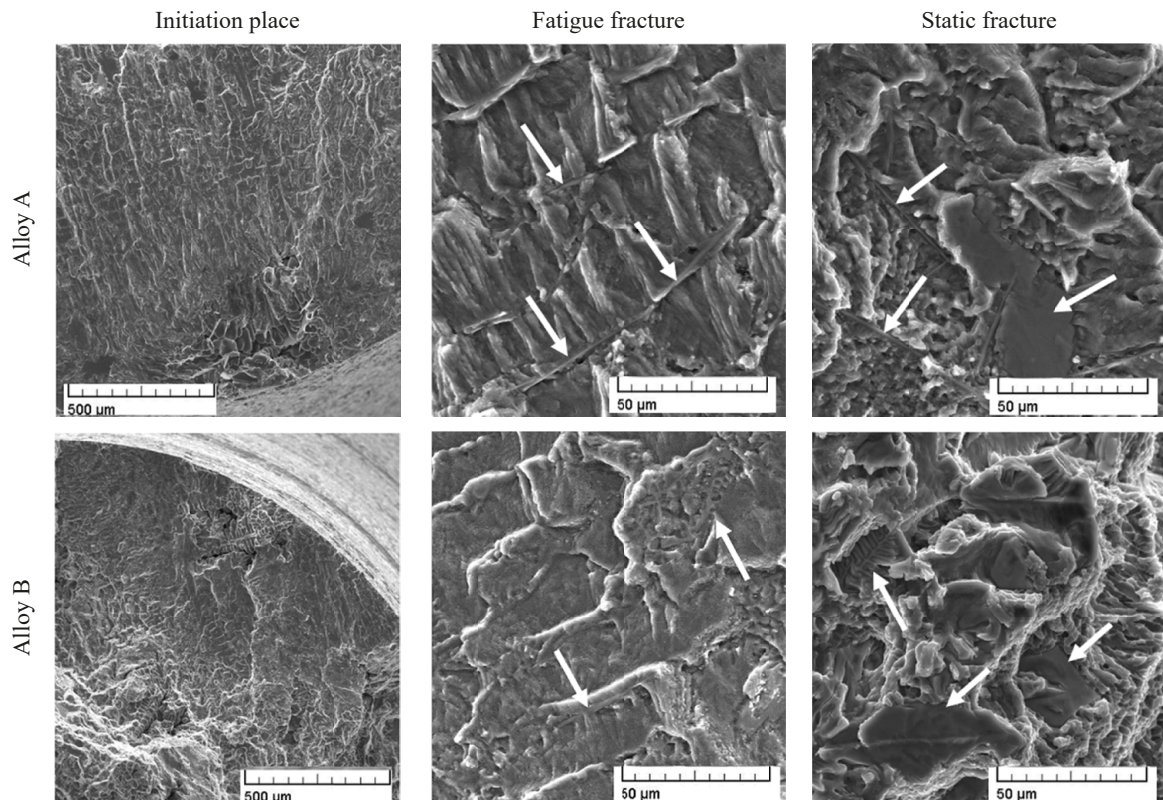


Fig. 8. Fractography analysis of fatigue and static fracture at the same stress amplitude of 88 MPa, Fe-rich phases arrowed; SEM

EDX analysis was used to declare the presence of phases in the fatigue fracture region during the fractographic evaluation (Fig. 9). In the fatigue fracture regions, the Fe phases were observed as thin needles or long platelets, based on their orientation with respect to the fatigue crack propagation. This excluded the possibility, that the crack preferentially propagated along a certain morphology and orientation of these phases.

5. Conclusion

This study investigates the effect of Mn on the microstructure, corrosion, and fatigue properties of secondary A357 alloy. According to the experimental results and analysis performed can be concluded that:

- All experimental alloys have comparable main microstructural constituents. The microstructure consists of α -phase,

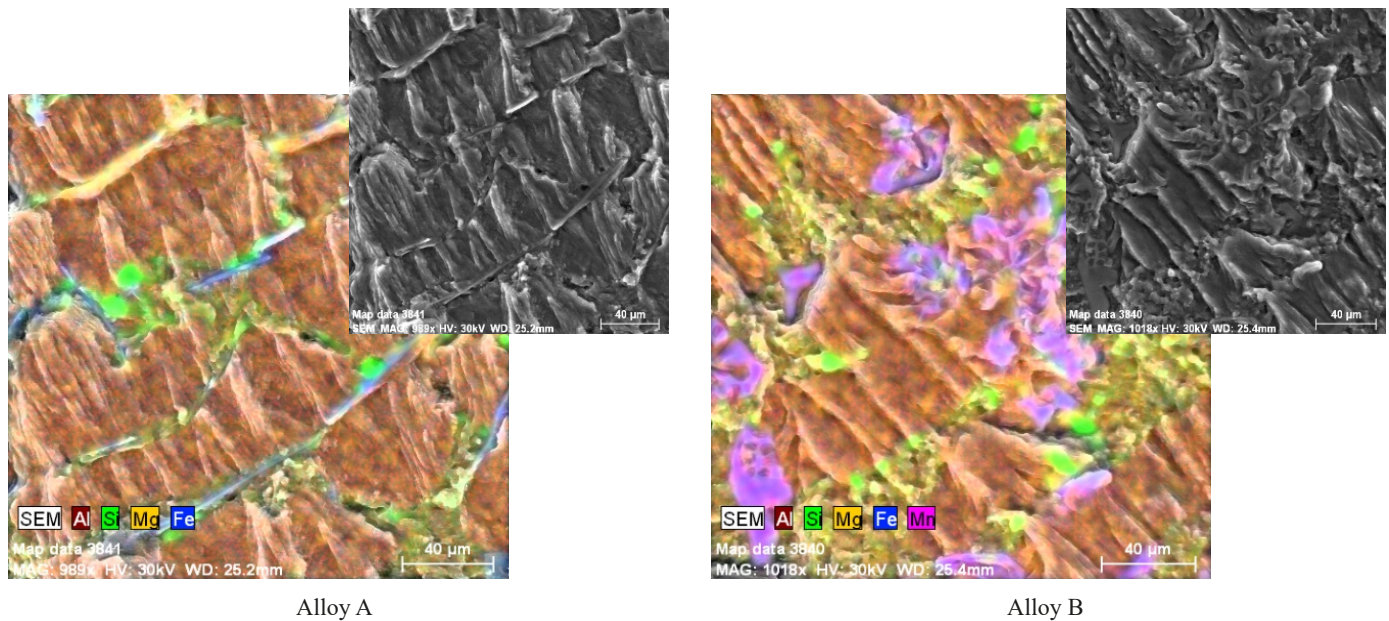


Fig. 9. EDX analysis of Fe-rich intermetallic phases on fatigue surface, SEM

eutectic, and intermetallic phases. The amount and chemical composition of intermetallic phases depend on the type of experimental alloy, but all of them contain Chinese script – Mg_2Si , skeleton-like $Al_{15}(FeMg)_2Si_2$ phases, Fe-needle-like Al_5FeSi phases. The alloy B with Mn addition contains $Al_{15}(FeMnMg)_3Si_2$ phases in the form of Chinese script or skeleton – like.

- The results of corrosion tests show that corrosion pits were created on the surface of the samples, preferably in areas of eutectic and Fe-rich phases. The Mn addition had no significant effect on the corrosion mechanism.
- Alloy B with higher Mn content and a higher number of Fe-rich phases exhibits a higher corrosion rate when compared to alloy A (0.027 vs 0.011).
- The results of fatigue life tests show a higher fatigue life for alloy B with Mn addition, however, due to the high porosity causing crack initiation in both alloys, it is not possible to prove with confidence that Mn has a positive effect on the fatigue life.
- In both experimental alloys, the fatigue fractures are characterized by the transcrystalline fatigue fracture of an Al-matrix with striations. The final fracture is characterized by transcrystalline ductile fracture of the matrix with dimple morphology.
- Since the fatigue life is determined by microstructural defects, the Fe-rich phases did not play a key role in crack initiation and propagation.

Acknowledgement

This work was supported under the project KEGA no. 004ŽU-4/2023, and project to support young researchers at UNIZA, ID of project 12715 – project leader Ing. Lenka Kuchariková

REFERENCE

- [1] M. Zamani. Al-Si Cast Alloys – Microstructure and Mechanical Properties at Ambient and Elevated Temperature. Licentiate thesis, Jönköping University, Jönköping (2015). ISBN 978-91-87289-08-8
- [2] J. Svobodova, M. Lunak, M. Lattner, Analysis of the Increased Iron Content on the Corrosion Resistance of the AlSi7Mg0.3 Alloy Casting. *Manufacturing Technology* **19** (6), 1041-1046 (2019). DOI: <https://doi.org/10.21062/ujep/415.2019/a/1213-2489/MT/19/6/104>
- [3] L. Kuchariková, et al., Quality Assessment of Al Castings Produced in Sand Molds Using Image and CT Analyses. *Journal of Materials Engineering and Performance* **28** (3), (2019). DOI: <https://doi.org/10.1007/s11665-019-04040-z>
- [4] E. Kantoriková, M. Kuriš, R. Patirčák, Heat treatment of Al-Si7Mg0.3 aluminium alloys with increased zirconium and titanium content. *Archives of Foundry Engineering* **21** (I. 2), 89-96 (2021). DOI: <https://doi.org/10.24425/afe.2021.136103>
- [5] <https://www.novelis.com/recycled-aluminium-as-key-enabler-of-decarbonization/>
- [6] L. Shehadeh, I. Jalham, The effect of adding different percentages of manganese (Mn) and copper (Cu) on the mechanical behavior of aluminum. *Jordan Journal of Mechanical and Industrial Engineering* **10** (1), 19-26 (2016).
- [7] V. Deev et al., Crystallization Behavior and Properties of Hypereutectic Al-Si Alloys with Different Iron Content. *Archives of Foundry Engineering* **20** (4), 101-107 (2020). DOI: <https://doi.org/10.24425/afe.2020.133355>
- [8] D. Závodská et al., The effect of iron content on fatigue lifetime of AlZn10Si8Mg cast alloy. *International Journal of Fatigue* **128**, (2019). DOI: <https://doi.org/10.1016/j.ijfatigue.2019.105189>.
- [9] D. Bolibruchová, L. Richtárech, Lukáš, Elimination of Iron Based Particles in Al-Si Alloy. *Archives of Foundry Engineering* **15** (1), 9-12 (2015). DOI: <https://doi.org/10.1515/afe-2015-0002>

- [10] L. Kuchariková et al., The Effect of the β -Al₅FeSi Phases on Microstructure, Mechanical and Fatigue Properties in A356.0 Cast Alloys with Higher Fe Content without Additional Alloying of Mn. *Materials* **14** (8), 1943 (2021). DOI: <https://doi.org/10.3390/ma14081943>
- [11] L. Kuchariková, et al., Role of Chemical Composition in Corrosion of Aluminum Alloys. *Metals* **8** (8), 581 (2018). DOI: <https://doi.org/10.3390/met8080581>
- [12] R. Arrabal, et al., Microstructure and corrosion behaviour of A356 aluminium alloy modified with Nd. *Materials and Corrosion* **66**, 535-541 (2015). DOI: <https://doi.org/10.1002/maco.201407674>
- [13] P. Biswas, et al., Effect of Mn Addition on the Mechanical Properties of Al-12.6Si Alloy: Role of Al₁₅(MnFe)₃Si₂ Intermetallic and Microstructure Modification. *Metals and Materials International* **27**, 1-15. (2019). DOI: <https://doi.org/10.1007/s12540-019-00535-5>
- [14] R. Podprocká, D. Bolibruchová, The Role of Manganese in the Alloy Based on Al-Si-Mg with Higher Iron Content. *Manufacturing Technology* **18**, 650-654 (2018). DOI: <https://doi.org/10.21062/ujep/155.2018/a/1213-2489/MT/18/4/650>
- [15] M. Pasternak, M. Brzeziński, Analysis and Evaluation of Effect of Manganese Content on Properties of EN AC 46000 Aluminum Alloy. *Journal of Casting & Materials Engineering* **3** (1), 14-18 (2019). DOI: <https://doi.org/10.7494/jcme.2018.3.1.14>
- [16] M. Mikolajčík, E. Tillová, L. Kuchariková, L. Pastierovičová, M. Chalupová, M. Uhrčík, Z. Šurdová, Effect of Higher Iron Content and Manganese Addition on the Corrosion Resistance of AlSi₇Mg_{0.6} Secondary Alloy. *Manufacturing Technology* **22**, 436-443 (2022). DOI: <https://doi.org/10.21062/mft.2022.057>
- [17] J. Esquié, R. K. Gupta, Simultaneous improvement of mechanical and corrosion properties of aluminium alloys. *Light metals 2016*. Chapter **26**. 151-156 (2016).
- [18] R. Arrabal, B. Mingo, A. Pardo, M. Mohedano, E. Matykina, I. Rodríguez, Pitting corrosion of rheocast A356 aluminium alloy in 3.5wt.% NaCl solution. *Corrosion Science* **73**, 342-355 (2013). DOI: <https://doi.org/10.1016/j.corsci.2013.04.023>
- [19] M. Tebaldini, C. Petrogalli, G. Donzella, G.M. La Vecchia, Estimation of Fatigue Limit of a A356-T6 Automotive Wheel in Presence of Defects. *Procedia Structural Integrity* **7**, 521-529 (2017). DOI: <https://doi.org/10.1016/j.prostr.2017.11.121>
- [20] L. Pastierovičová, L. Kuchariková, E. Tillová, M. Chalupová, M. Bonek, The Effect of Manganese on Fe-Rich Intermetallic Phases in Progressive Secondary AlSi₇Mg_{0.6} Alloy. *Applied Engineering Letters* **7** (3), 100-107 (2022). DOI: <https://doi.org/10.18485/aeletters.2022.7.3.2>
- [21] M. Lorusso, F. Trevisan, F. Calignano, M. Lombardi, D. Manfredi, A357 Alloy by LPBF for Industry Applications. *Materials (Basel)* **13** (7), 1488 (2020). DOI: <https://doi.org/10.3390/ma13071488>
- [22] L. Kuchariková et al 2021 IOP Conf. Ser.: Mater. Sci. Eng. 1178 012037.
- [23] P. Mikołajczak, L. Ratke, Three Dimensional Morphology of β -Al₅FeSi Intermetallics in AlSi Alloys. *Arch. Foundry Eng.* **15**, 47-50 (2015). DOI: <https://doi.org/10.1515/afe-2015-0010>